Fusion of ^{28}Si nuclei at 12.4, 19.7, and 30.0 MeV/nucleon

R. J. Meijer,[1,2,*] P. F. Box,[1] P. Decowski,[1,†] E. Gierlik,[1,‡] R. Kamermans,[1] G. J. van Nieuwenhuizen,[1] K. A. Griffioen,[3,1] H. W. Wilschut,[4] A. Giorni,[5] C. Morand,[5] A. Demeyer,[6] and D. Guinet[6]

[1]*R. J. Van de Graaff Laboratory, Rijksuniversiteit Utrecht, Princetonplein 5, 3508 TA Utrecht, The Netherlands*

[2]*Gesellschaft für Schwerionenforschung mbH, Planckstrasse 1, D-6100 Darmstadt 11, Germany*

[3]*Department of Physics, University of Pennsylvania, Philadelphia, Pennsylvania 19104*

[4]*Kernfysisch Versneller Instituut, Zernikelaan 25, 9747 AA Groningen, The Netherlands*

[5]*Institut des Sciences Nucléaires, Av. des Martyrs 53, F-38026 Grenoble CEDEX, France*

[6]*Institut de Physique Nucléaire, Université Claude Bernard, 43 bd du 11 Novembre 1918, F-69622 Villeurbanne CEDEX, France*

(Received 21 January 1991)

Detailed angular distributions of protons and α particles detected in coincidence with evaporation residues have been measured for the reaction ^{28}Si+^{28}Si at 12.4, 19.7, and 30.0 MeV/nucleon. We have separated these angular distributions into pre-equilibrium and evaporation components. The invariant velocity distributions of pre-equilibrium protons are typical for nucleons emitted by jetting processes, while the distributions of pre-equilibrium α particles are typical for particles produced in breakup reactions. The charge and energy balance in the reaction allows us to reconstruct the average properties of the compound nucleus and to deduce the effects of the reaction dynamics. At 12.4 MeV/nucleon only a few pre-equilibrium light particles are emitted prior to fusion, whereas at 19.7 and 30.0 MeV/nucleon hot nuclei are formed in breakup-fusion reactions. All of our results can be fully explained assuming that compound nuclei do not produce evaporation residues if their excitation energy is above 4.3 MeV/nucleon.

I. INTRODUCTION

The study of the formation and decay of highly excited nuclei has generated great interest over the past few years [1,2]. Ever since emulsion experiments showed multiple-heavy-ion exit channels, the phenomenon of multifragmentation (the instantaneous disintegration of a highly excited and compressed nucleus into many intermediate-mass fragments) has received much attention. However, the experimental evidence for multifragmentation seems to be inconclusive at best. On the theoretical side the situation is similar. Multiple-heavy-ion exit channels can be predicted with dynamical models that follow the trajectories of nucleons inside the colliding nuclei as well as with statistical models that contain minimal information on nuclear interactions but assume equilibrium prior to the decay of a hot nucleus formed during the heavy-ion collision [3,4].

One can roughly divide the statistical models into two classes: those that treat the decay of a highly excited nucleus as an instantaneous process, multifragmentation, or those that treat it as a sequential process, evaporation. Despite the large differences in the assumptions on which these models are based, the results are similar and show the same features as inclusive measurements. Recently, the similarity in the results of these two types of calculations has been discussed by Friedman [4]. His work indicates that high multiplicities of intermediate-mass fragments are not a clear experimental signature of the multifragmentation phenomenon.

On the other hand, experiments with heavy ions show that the cross section of decay products historically associated with fusion, evaporation residues (ER's) and fission fragments, vanishes at beam energies between 30 and 40 MeV/nucleon (see, e.g., Ref. [5]). Since the excitation energy of fully fused systems in heavy-ion collisions at these beam energies is high, on the order of the nuclear binding energy, multifragmentation of the highly excited systems was proposed as one of the explanations. According to the authors of Ref. [5], however, the reaction dynamics hinders the formation of fused nuclei. Unstudied so far is the relative change in the strength of the fission and ER exit channels. Previous experiments were only sensitive to one type of decay product, fission fragments in heavy systems, and ER's in light systems. However, the fission probability for light nuclei increases dramatically at high excitation energies, whereas the fission process of heavy nuclei at high excitation energies is hindered, since the fission barrier is increased by the fast evaporation of neutrons.

One of the steps in the systematic investigation of highly excited nuclei is the determination of the extreme conditions under which they decay conventionally by evaporation or fission. At what beam energies does evaporation still persist, and to what nuclear excitation energy does this correspond? The two essential quantities needed for such an exploration, the average excitation energy and the mass of the compound nucleus (CN) produced in the incomplete-fusion reaction, can be obtained from relatively simple measurements of ER's in coincidence with light particles (LP's) [6].

This paper presents the results of an experimental study of the formation and decay of the CN produced in fusionlike reactions of ^{28}Si+^{28}Si at 12.4, 19.7, and 30.0 MeV/nucleon. The beam energies were chosen such that CN's could be formed with excitation energies of about 3,

5, and 7.5 MeV/nucleon, if all of the available c.m. kinetic energy went into excitation energy. The highest excitation energy is close to the nuclear binding energy per nucleon and is therefore almost sufficient for a complete disintegration of the CN [1]. Since we are colliding two equal nuclei, these excitation energies are reached with a minimal relative velocity of the projectile and target nucleus. The effects of incomplete fusion are thus smaller than in asymmetric reactions in which similar hot nuclei are formed. Therefore, if pre-equilibrium particle emission in $^{28}Si+^{28}Si$ reactions does not significantly hinder the formation of highly excited nuclei, then it is very probable that we will see a change in the decay mode of hot nuclei from the evaporation of LP's to other modes as we increase the beam energy of the reaction.

The symmetry of the velocity distributions in the c.m. system, which is a consequence of colliding two equal nuclei, is advantageous for the measurements as well as for the analysis. The actual choice of the element Si as projectile and target was based upon three further requirements: (1) the fused system must decay (at moderate excitation energies) primarily by LP evaporation, (2) one should be able to manufacture clean, and isotopically pure targets of the element, and (3) a gaseous chemical compound of the element should exist for use in the ECR injectors.

Applied to the present data, the method of Ref. [6] enabled us to obtain a better picture of the fusion process and to find clear evidence for a limiting excitation energy above which no CN decays to an ER. We have developed a Monte Carlo model of the formation and decay of the CN, which is fully consistent with all observables, provided we assume that nuclear decay by particle evaporation is limited to excitation energies below 4.3 MeV/nucleon.

In the next section of this article the experimental setup is described. Section III reports on the measurements of the inclusive heavy-ion (HI) spectra from which the ER cross sections at the three beam energies were determined. Section IV describes the analysis of the LP distributions, which where measured in coincidence with ER's. Section V presents a Monte Carlo model for the $^{28}Si+^{28}Si$ reactions that reflects the results of Sec. IV and which is used to check our conclusions with data. A summary can be found in Sec. VI.

II. EXPERIMENTAL SETUP

Figure 1 shows the experimental setup used in the exclusive measurements with the 19.7 and 30.0 MeV/nucleon beams. A HI detector consisting of a 10 cm long ionization chamber and a 1000 μm Si detector was placed at angles between 3° and 6° with respect to the beam. The ionization chamber was filled with CF_4 at a pressure of 21.8 Torr in the 12.4 MeV/nucleon experiment and at 15.0 Torr in the 19.7 and 30.0 MeV/nucleon experiments. The gas was continuously refreshed. Under these conditions we were able to extract the ion energy and charge. The beam axis and the HI detector define the $\phi=0°$ plane for our setup. Polar angles θ are measured from the beam direction with positive angles lying on the same side of the beam as the HI detector and negative angles opposite to this. A monitor detector, used for normalization purposes, was placed at $\theta=-3°$. LP's were detected with 16 telescopes of the Utrecht multidetector system [7,8]. Each telescope consisted of a 150 μm Si detector and a 3 cm CsI(Tl) crystal with photodiode readout. For the 12.4 MeV/nucleon coincidence measurements, LP's were detected with four three-

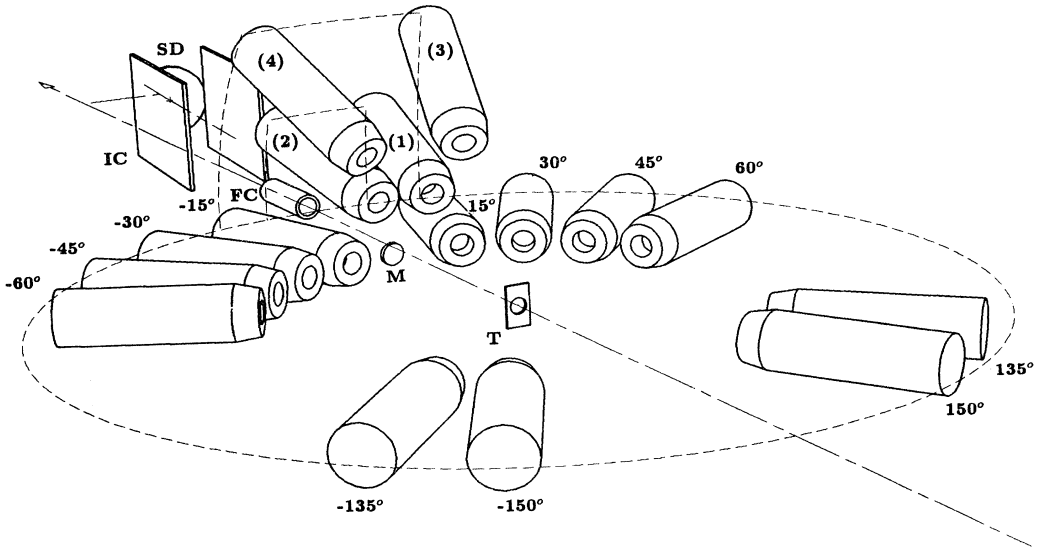

FIG. 1. Detector configuration used in the 19.7 and 30.0 MeV/nucleon $^{28}Si+^{28}Si$ experiments. M is the beam monitor placed at 3°, FC is the Faraday cup, and T is the target. A heavy-ion detector consisting of a ionization chamber IC and a silicon detector SD was placed at 3°. All other detectors were Si-CsI telescopes for LP detection. The angle θ of each in-plane telescope is given. The positive values correspond to $\phi=0°$ angles, the negative to $\phi=180°$ angles.

element telescopes, consisting of two Si detectors and a CsI detector. In addition, two conventional three-element and two-element Si telescopes were used. The HI detector, in this case, was a prototype of the detector used in the experiments at the higher beam energies. By rotating the setups we could measure the LP energy distribution at 24 angles at 12.4 MeV/nucleon and at 32 angles at the two higher beam energies. All of the detectors in the 12.4 MeV/nucleon experiment were positioned in the $\phi=0°$ plane, whereas in the experiments at 19.7 and 30.0 MeV/nucleon eight angles were out of plane.

During and after the experiments, energy calibrations with α sources and a precision pulser were performed. The absolute normalization of the total ER cross section in the 12.4 MeV/nucleon experiment was obtained from systematics and at 19.7 and 30.0 MeV/nucleon via the elastic scattering cross section for ^{28}Si+^{197}Au, which was measured with the HI detector at the same beam energies. The absolute normalization has an accuracy of 20%. The energy calibration of the CsI detectors is described in Ref. [9]. The ^{28}Si targets used were produced via a novel procedure that yields clean and strong self-supporting targets [11]. Before and after each experiment the thickness and impurity of the targets was determined from the energy spectrum of elastically scattered α and ^{12}C particles, which were accelerated by the Utrecht tandem Van de Graaff accelerator. The thickness of the targets used in the experiments varied between 315 and 367 μg/cm^2. The targets were contaminated mainly by C and O. The total concentration of contaminants was less than 3% of the number of Si atoms at the beginning of the experiments, and typically 10% at the end. No effects of these impurities appeared in the analyzed data.

With the setups described above, we have measured full angular distributions of LP's ($p,d,t,^3$He,α) in coincidence with HI's at forward angles ($3° \leq \theta_{HI} \leq 6°$). Inclusive HI angular distributions $3° < \theta_{HI} < 20°$ were also measured at all beam energies with the LP detectors removed from the setup. The inclusive ER distributions at 12.4 MeV/nucleon were measured with a detector that also determines the mass number of the particles [10]. However, its solid angle was too low to be used in the coincidence experiments.

Our data set consisted of coincidences between a LP telescope and the HI detector, coincidences between any pair of LP detectors, and of scaled-down singles in the LP, monitor, and HI detectors. Tables I and II give an overview of the data measured. The dead time of the acquisition system was kept around 10%.

III. INCLUSIVE RESULTS

In Figs. 2, 3, and 4 inclusive HI velocity-spectra measured at 12.4, 19.7, and 30.0 MeV/nucleon are shown as a function of Z_{HI}. For $Z_{HI} \geq 15$ the yield and the width of the Maxwellian shaped ER laboratory velocity distribution can be determined easily. Near the velocity of the c.m. system, where this distribution reaches its maximum, there is only a small contribution from nuclei created in peripheral or deep-inelastic processes. For

TABLE I. Overview of the ^{28}Si+^{28}Si exclusive LP-HI data.

Beam energy (MeV/nucleon)	12.4	19.7	30.0
Number of LP detectors	8	16	
Number of HI detection angles	1	2	
Number of LP detection angles	24	32	
Number of LP-HI pairs	24	64	
HI detection angles θ (deg), $\phi=0°$	5	4 6	3 6
LP detection angles θ (deg), $\phi=0°$	15 25 35 45 55 65 75 95 115 150 160 169	15 21 30 36 60 66 135 141	45 51 150 156
LP detection angles θ (deg), $\phi=180°$	5 12.5 16.1 22.2 25.8 32.2 35.8 45.3 55 65 110 160	9 15 24 30 54 60 129 135	39 45 144 150
LP detection angles (deg), (θ,ϕ)		(16.7, 64.0) (33.2, 65.9) (16.7, 116.0) (33.2, 114.1) (31.2, 105.2) (36.1, 58.2)	(15.1, 95.6) (20.1, 50.0)
HI charge numbers	9, . . . ,24	6, . . . ,21	8, . . . ,21
LP	$p,d,t,^3$He,α	$p,d,t,^3$He,α	

TABLE II. Overview of $^{28}Si+^{28}Si$ inclusive HI data.

Beam energy	(MeV/nucleon)	12.4	19.7	30.0
HI angles	(deg)	5,6,7,8 9,10,11,12, 13,14,15,16 17,18,19	3,5,7,9 10,11,12,13, 18,23	3,4,6,7 8,9,10,11, 12,16,20
HI charge numbers	Z	9–24	6–21	8–21
HI mass numbers	A	18–47		

$Z_{HI} < 15$, however, the spectra contain overlapping contributions from quasielastic, deep-inelastic, and fusionlike processes. Our decomposition of these spectra into these components follows the method outlined in Ref. [12]. From the amplitudes and widths of the inclusive ER velocity distributions, we determined the angular dependence of the differential ER cross section $d^2\sigma_{ER}/dZ_{ER}d\Omega$ (see, e.g., Fig. 5). Then, via an integration over a solid angle, we obtained the ER cross section as a function of Z_{ER}, i.e., $d\sigma_{ER}/dZ_{ER}$, as shown in Fig. 6. Figures 5 and 6 also show the results of Monte Carlo calculations, which will be discussed in Sec. V.

The cross sections $d\sigma_{ER}/dZ_{ER}$, measured at 19.7 MeV/nucleon, peak at a lower value ($Z_{ER}=14$) than at 12.4 MeV/nucleon ($Z_{ER}=19$). A decrease of the most probable Z_{ER} value with higher incident energies can be explained as an effect of the higher excitation energy of the CN, which results in a longer decay chain and, hence,

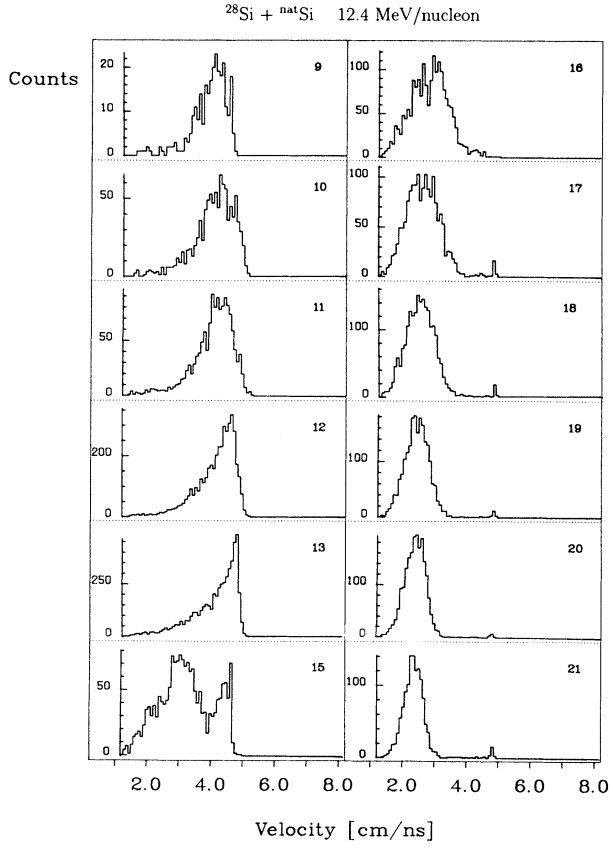

FIG. 2. HI velocity spectra measured at 5° for the $^{28}Si+^{28}Si$ reaction at 12.4 MeV/nucleon. The charge of the HI is give in the upper right-hand corner.

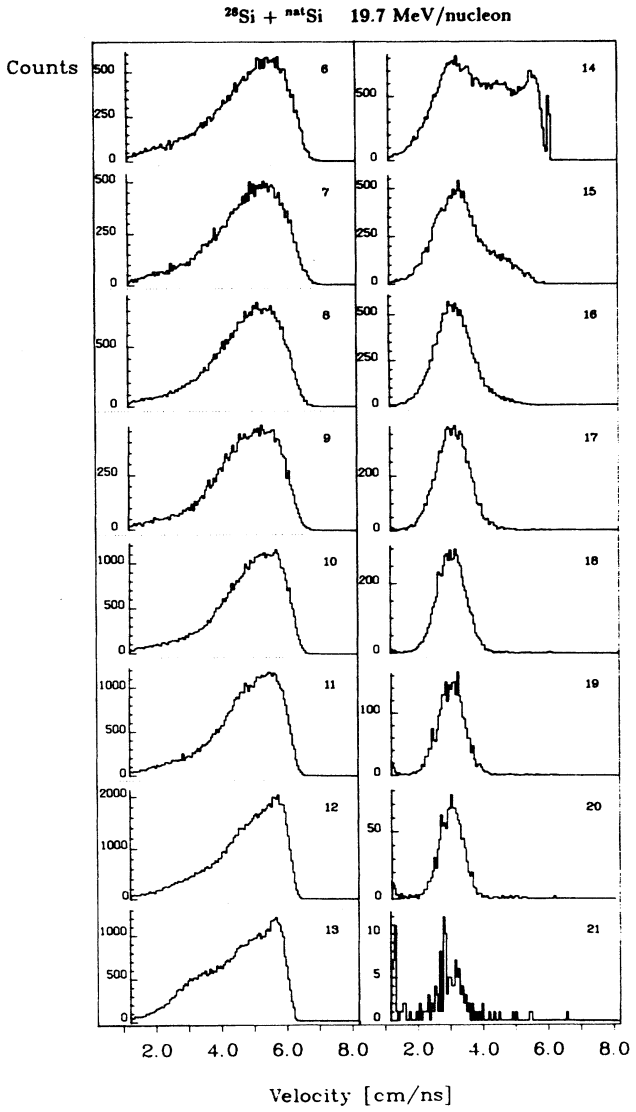

FIG. 3. Sum of the HI velocity spectra measured at 4° and 6° for the $^{28}Si+^{28}Si$ reaction at 19.7 MeV/nucleon. The charge of the HI is given in the upper right-hand corner.

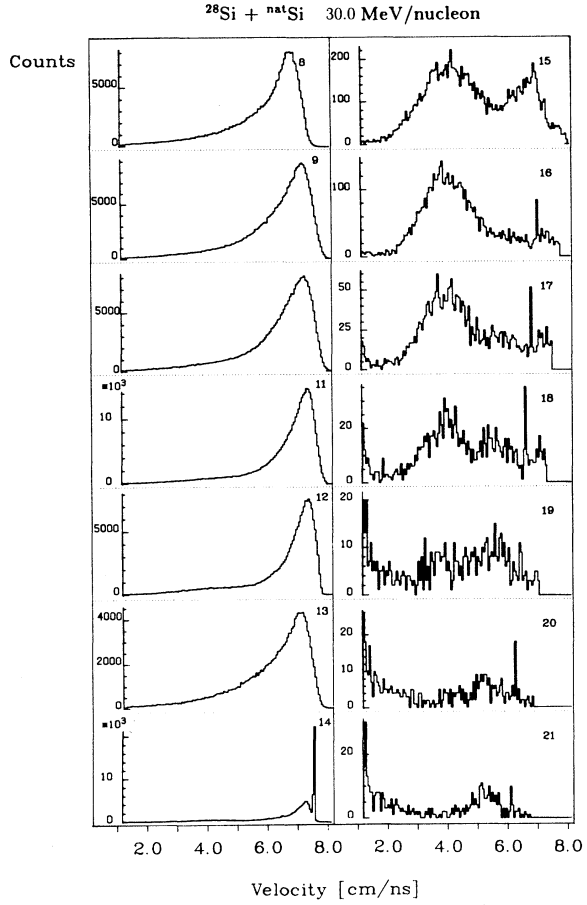

FIG. 4. Sum of the HI velocity spectra measured at 3° and 6° for the ^{28}Si+^{28}Si reaction at 30.0 MeV/nucleon. The charge of the HI is given in the upper right-hand corner.

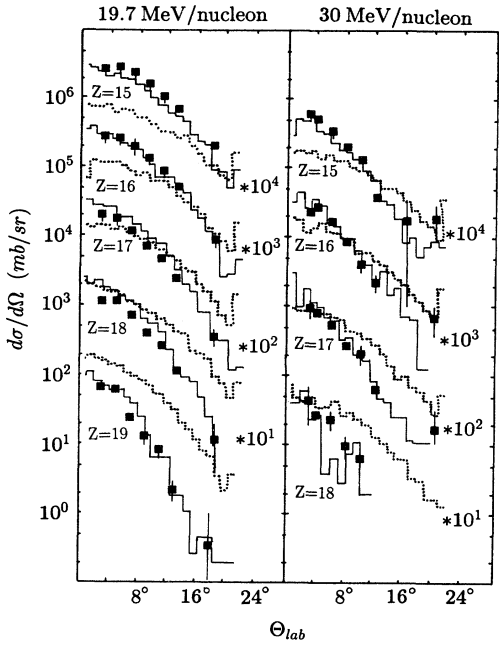

FIG. 5. Inclusive evaporation residue cross sections for ^{28}Si+^{28}Si reactions at 19.7 and 30.0 MeV/nucleon as a function of detection angle for various Z_{ER}. The solid and dotted histograms show the results of the Monte Carlo and the alternative Monte Carlo model, respectively (see Sec. V).

a smaller average charge of the ER. This trend is reproduced by the statistical-model code CASCADE [13]: the most probable Z_{ER} value lies at $Z_{ER}=20$, 17, and 14 for complete fusion reactions of ^{28}Si+^{28}Si at 12.4, 19.7, and 30.0 MeV/nucleon, respectively. To first order, preequilibrium emission does not change these values. The average initial change of the CN in this case is expected to be smaller, but so too is the excitation energy. The measured ER charge distribution at 30.0 MeV/nucleon does not follow the expected trend. At this energy the most probable ER charge, $Z_{ER}=15$, is close to the value found at 19.7 MeV/nucleon.

In Fig. 7 the total ER cross section for ^{28}Si+^{28}Si reactions is plotted as a function of the beam energy. The triangles are the cross sections reported in Ref. [14]. The circles are our own data (there is no point at 12.4 MeV/nucleon, since we determined our ER cross section at this energy from systematics). The solid line shows the calculated fusion cross section corresponding to $l_{crit}=44\hbar$ [15]. The dashed line describes the ER contribution to the fusion cross section as calculated by the statistical model GEMINI [16]. This model is also able to calculate the cross sections of fission products. Above 20.0 MeV/nucleon the measured ER cross sections are decreasing much faster than either a smooth extrapolation of the data from lower energies or the calculations would indicate. The ER cross section at 30.0 MeV/nucleon is a about a factor of 10 lower than one might expect from systematics.

The rapid decrease of the cross section for fusion products with rising bombarding energies is known for other reactions as well, most notably for ^{40}Ar-induced reactions (see, e.g., [17–20]). This phenomenon can be explained by the concept of a maximum excitation energy (per nucleon) that a nucleus can sustain [19,21].

IV. EXCLUSIVE RESULTS

In this section we present the angular distributions of LP's measured in coincidence with ER's. Combining the LP data with the information we have on the ER's allows us to deduce some of the properties of the CN's and of the fusion mechanism.

A. Off-line analysis

In the off-line analysis of the exclusive LP-HI measurements, ER's were identified by gates on the HI data. Then, for each detector angle, energy spectra of the coincident protons and α particles were generated.

In the analysis of the exclusive data taken at 12.4 MeV/nucleon ER's with $Z_{ER}\geq 15$ were identified by a

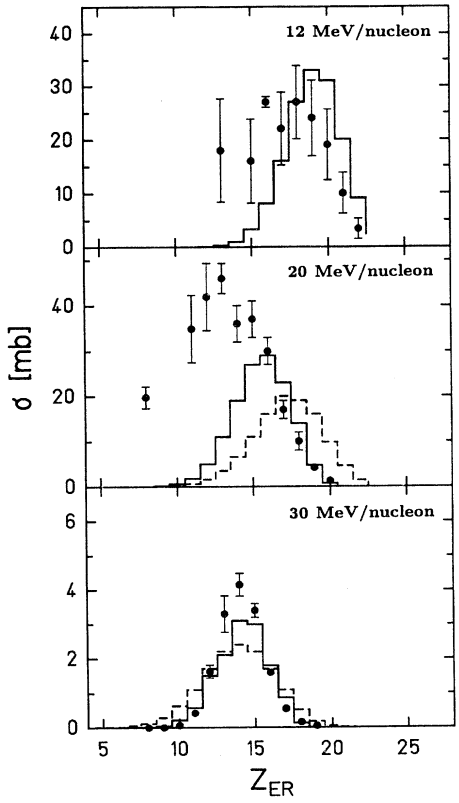

FIG. 6. Inclusive evaporation residue cross sections for $^{28}Si+^{28}Si$ reactions at 12.4, 19.7, and 30.0 MeV/nucleon as a function of Z_{ER}. The experimental results are indicated by the closed points, the solid and dotted histograms show the results of the Monte Carlo and the alternative Monte Carlo model, respectively (see Sec. V).

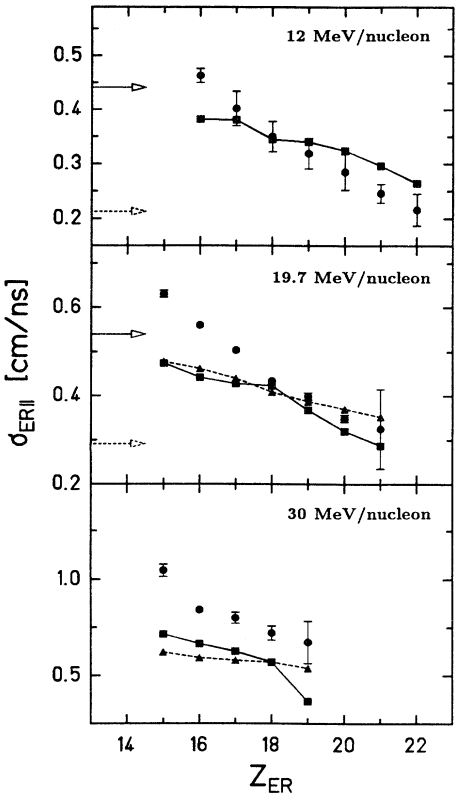

FIG. 8. Widths of the ER velocity distributions measured in the $^{28}Si+^{28}Si$ experiments at 12.4, 19.7, and 30.0 MeV/nucleon. The circles represent the experimental results, the squares connected with the solid lines and the triangles connected with the dashed lines represent the results of the Monte Carlo and the alternative Monte Carlo model, respectively (see Sec. V). The widths obtained from the analysis of exclusive proton and α distributions are indicated by the full and dashed arrows, respectively (see Sec. IV).

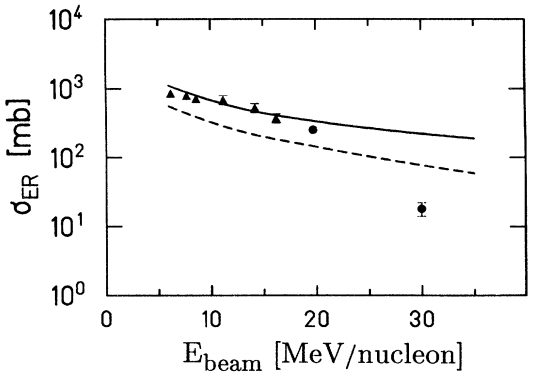

FIG. 7. Evaporation residue cross sections for $^{28}Si+^{28}Si$ reactions as a function of the beam energy per nucleon. The triangles represent the measurements of Ref. [14], the circles are from this work. The solid line gives the fusion cross section calculated for $l_{crit}=44\hbar$. The dashed line shows the calculated ER cross sections for the complete fusion process (see text).

two-dimensional gate on the ΔE and E signals in the HI detector. The inclusive HI spectra presented in Fig. 2 show that this gate selects almost uniquely all ER's; only a small admixture of HI's from peripheral reactions are included. However, the prototype HI detector used for the coincidence experiments had a Z resolution of about 1 charge unit, and therefore some HI's with $Z_{HI}=14$, mostly from peripheral reactions, were selected too.

In the experiments at 19.7 and 30.0 MeV/nucleon the resolution of the HI detector was much improved. The conditions $Z_{HI} \geq 15$ and

$$v_{c.m.} - v_{FWHM} < v_{HI} < v_{c.m.} + v_{FWHM}$$

were used to select ER's. The quantity v_{FWHM} is the full width at half maximum (FWHM) of the inclusive ER velocity distribution. The experimental widths of the ER velocity distribution, from which $v_{FWHM}=2.35\sigma_{ER\|}$ is calculated, are shown as a function of Z_{ER} in Fig. 8. Since approximately 50% of all HI's have $Z_{ER} \geq 15$ (see Fig. 6), these gates select about half of the ER's formed at 19.7 and 30.0 MeV/nucleon.

In the exclusive experiments the HI detector, having an opening angle of 1.8°, was positioned at 5° in the experiment at 12.4 MeV/nucleon, at 4° and 6° in the experiment at 19.7 MeV/nucleon and at 3° and 6° in the experiment at 30.0 MeV/nucleon. These angles were chosen such that the angular range of maximum $d\sigma_{\rm ER}/d\theta$ was covered. For each combination of angles between the LP telescopes and the HI detector (see Table I) LP energy spectra were generated. For the 19.7 MeV/nucleon data, only the results based on the measurements of LP's coincident with ER's measured at the 4° HI-detector setting are presented, since we obtain identical results from the analysis of the LP spectra measured in coincidence with ER's at the 6° setting. To increase the statistics of the LP spectra in the 30.0 MeV/nucleon experiment, the LP spectra measured in coincidence with ER's detected at 3° and 6° were summed. We have checked that this improves the statistical accuracy without changing the results. The analysis presented in this paper is focused on the results obtained for protons and α particles, since the summed yield of all other particles measured was at least a factor of 10 smaller, and omission of these does not affect the determination of the average charge and excitation energy of the CN's [6].

B. Description of exclusive LP spectra

In this work we have used the coincidence moving source model from Ref. [22] to describe the exclusive LP yield. The model decomposes the LP yield into a preequilibrium and an evaporation part and takes the kinematical constraint of the coincidence requirement into account. The parameters of the model are determined by a fit to the experimental LP distributions. In symmetric reactions the LP distributions have a fore-aft symmetry in the c.m. system, which greatly reduces the number of free parameters in the model.

In our analysis we made a modification in the evaporation part of the expressions derived in Ref. [22], and, in view of the identical role played by the projectile and target nucleus in the fusion process, we extended the approach of Ref. [22] to include a target source of preequilibrium particles. We have taken the following form for the distribution of evaporated particles in the c.m. system of an excited nucleus:

$$\frac{d^2\sigma}{dE_{\rm c.m.}d\Omega_{\rm c.m.}} \propto \frac{\sqrt{E_{\rm c.m.}}\,e^{-E_{\rm c.m.}/T}}{1+e^{-(E_{\rm c.m.}-E_C)/T_C}} \frac{1}{(\sin^2\theta_{\rm c.m.}+k\cos^2\theta_{\rm c.m.})^{1/2}} , \tag{1}$$

in which $E_{\rm c.m.}$ is the c.m. kinetic energy of the emitted particle, $\theta_{\rm c.m.}$ is the c.m. polar angle of the evaporated particle, T is the spectrum slope parameter, and E_C and T_C determine the shape of the Coulomb barrier transmission factor. The angular dependence of the c.m. LP distribution is governed by k: e.g., for $k=1$ the c.m. distribution is isotropic, while for $k=0$ the c.m. distribution has the $1/\sin\theta_{\rm c.m.}$ shape. In the present case the ER is much heavier than the LP, and therefore we have neglected the c.m. kinetic energy of the ER in $E_{\rm c.m.}$. With this form for the c.m. distribution of evaporated particles, we can interpret T under certain circumstances as the initial temperature of the CN; see Sec. IV G. We derive the coincidence cross section by assuming that the residues are normally distributed about the recoil velocity produced by the emission of the observed light particle. The corresponding form of the coincidence cross section is quite insensitive to exactly when in the chain the light particle is emitted [22]. As in Ref. [22] we find an expression for the laboratory distribution of evaporated particles with kinetic energy E_L measured in coincidence with an ER:

$$\frac{d^3\sigma_E}{dE_L d\Omega_L d\Omega_{\rm ER}} = N_E \left[\frac{E_L}{E_{\rm c.m.}}\right]^{1/2} \frac{\sqrt{E_{\rm c.m.}}\,e^{-E_{\rm c.m.}/T}}{1+e^{-(E_{\rm c.m.}-E_C)/T_C}} \frac{1}{[k+(1-k)(E_L/E_{\rm c.m.})\sin^2\theta_L]^{1/2}} \times e^{-v_0^2/(2\sigma_{\rm ER}^2)} \left[(\sigma_{\rm ER}^3+\sigma_{\rm ER}p^2)\Phi\left[\frac{p}{\sigma_{\rm ER}}\right] e^{p^2/(2\sigma_{\rm ER}^2)} + p\sigma_{\rm ER}^2\right] , \tag{2}$$

where N_E is a normalization factor and $\sigma_{\rm ER}$ is the width of the ER laboratory velocity distribution. We introduce

$$\epsilon = \frac{A}{A_P+A_T-A} , \tag{3}$$

in which A is the ejectile mass number, A_P and A_T are the projectile and target mass numbers, and we make use of the relation

$$E_{\rm c.m.} = \tfrac{1}{2}m(v_{\rm CN}^2+v_L^2-2v_L v_{\rm CN}\cos\theta_L) , \tag{4}$$

to compute the c.m. energy of the ejectile. In this expression $v_{\rm CN}$ is the average laboratory velocity of the ER (for symmetric reactions $\mathbf{v}_{\rm CN}=\mathbf{v}_{\rm c.m.}$) and v_L is the laboratory velocity of the evaporated particle. v_L can be calculated from the measured energy. The quantity p in Eq. (2) is expressed by

$$p = \cos\theta_{\rm ER}[(1+\epsilon)v_{\rm CN}-\epsilon v_L\cos\theta_L] - \epsilon v_L\sin\theta_L\sin\theta_{\rm ER}\cos(\phi_L-\phi_{\rm ER}) , \tag{5}$$

with θ_L and $\theta_{\rm ER}$ the laboratory polar angle of the LP and ER, ϕ_L and $\phi_{\rm ER}$ their laboratory azimuthal angles. v_0 is also used in Eq. (2) and is given by

$$v_0^2 = (1+\epsilon)^2v_{\rm CN}^2+\epsilon^2v_L^2-2\epsilon(1+\epsilon)v_{\rm CN}v_L\cos\theta_L . \tag{6}$$

Finally, the function $\Phi(x)$ is

$$\Phi(x)=\left[\frac{\pi}{2}\right]^{1/2}\left[1+\mathrm{erf}\left[\frac{x}{\sqrt{2}}\right]\right], \tag{7}$$

where erf is the error function. Note that the last term in Eq. (5) is the source of the asymmetry in the yield for particles detected at the same ($\phi_L=0°$) and opposite ($\phi_L=180°$) side of the beam with respect to the ER detector.

Assuming a Gaussian velocity distribution centered at the projectile velocity $\mathbf{v}_P$ for pre-equilibrium particles of mass m emitted from the projectile, we find

$$\frac{d\sigma}{d\mathbf{v}}\propto\exp[-(\mathbf{v}-\mathbf{v}_P)_\perp^2/(2\sigma_\perp^2/m^2)]\times\exp[-(\mathbf{v}-\mathbf{v}_P)_\parallel^2/(2\sigma_\parallel^2/m^2)], \tag{8}$$

with $\sigma_\parallel$ and $\sigma_\perp$ the parallel and perpendicular widths of the momentum distribution. Assuming that the pre-equilibrium particle is emitted from the projectile with mass A_P prior to fusion with the target, the exclusive distribution of pre-equilibrium particles emitted from a source with projectile velocity is [22]

$$\frac{d^3\sigma_P}{dE_L d\Omega_L d\Omega_{\mathrm{ER}}}=N_{\mathrm{PE}}\left[\frac{2E_L}{m^3}\right]^{1/2} e^{-(\mathbf{v}_L-\mathbf{v}_P)_\perp^2/(2\sigma_\perp^2/m^2)} e^{-(\mathbf{v}_L-\mathbf{v}_P)_\parallel^2/(2\sigma_\parallel^2/m^2)} e^{-\nu^2 v_0^2/(2\sigma_{\mathrm{ER}}^2)} \times\left[(\sigma_{\mathrm{ER}}^3+\sigma_{\mathrm{ER}}p^2)\Phi\left[\frac{p}{\sigma_{\mathrm{ER}}}\right]e^{p^2/(2\sigma_{\mathrm{ER}}^2)}+p\sigma_{\mathrm{ER}}^2\right], \tag{9}$$

in which N_{PE} is a normalization factor. Furthermore,

$$\mu=\frac{A}{A_P-A}, \tag{10}$$

$$\nu=\frac{A_P-A}{A_P+A_T-A}, \tag{11}$$

$$\mathbf{v}_0=(1+\mu)\mathbf{v}_P-\mu\mathbf{v}_L, \tag{12}$$

and

$$p=\cos\theta_{\mathrm{ER}}[\nu(1+\mu)v_P-\mu\nu v_L\cos\theta_L]-\mu\nu v_L\sin\theta_L\sin\theta_{\mathrm{ER}}\cos(\phi_L-\phi_{\mathrm{ER}}). \tag{13}$$

We can derive the expression that describes the distribution of target pre-equilibrium particles in coincidence with ER's in a similar way:

$$\frac{d^3\sigma_T}{dE_L d\Omega_L d\Omega_{\mathrm{ER}}}=N_{\mathrm{PE}}\left[\frac{2E_L}{m^3}\right]^{1/2} e^{-(\mathbf{v}_L-\mathbf{v}_T)_\perp^2/(2\sigma_\perp^2/m^2)} e^{-(\mathbf{v}_L-\mathbf{v}_T)_\parallel^2/(2\sigma_\parallel^2/m^2)} e^{-\nu^2 v_0^2/(2\sigma_{\mathrm{ER}}^2)} \times\left[(\sigma_{\mathrm{ER}}^3+\sigma_{\mathrm{ER}}p^2)\Phi\left[\frac{p}{\sigma_{\mathrm{ER}}}\right]e^{p^2/(2\sigma_{\mathrm{ER}}^2)}+p\sigma_{\mathrm{ER}}^2\right] \tag{14}$$

with $\mathbf{v}_T$ (=0) the laboratory velocity of the target nucleus. Note that all parameters of the target and the projectile component are identical for the symmetric ^{28}Si+^{28}Si system.

We have fit the sum of Eqs. (2), (9), and (14) to the exclusive distributions of protons and α particles using the χ^2 minimization routine MINUIT [23]. The fitted parameters are given in Table III. The errors, presented in parentheses, are obtained from MINUIT and are given in units of the last decimal of the parameter value. In the fits we have set θ_{HI} equal to the central angle of the HI detector at 12.4 and 19.7 MeV/nucleon, while its value at 30.0 MeV/nucleon is the average of the central angles for two HI detector settings. To reduce the number of free parameters at 30.0 MeV/nucleon, the values of σ_{ER}, E_C, and T_C obtained at 19.7 MeV/nucleon were used. The parameters μ and ν were kept fixed at their theoretical value. We will now discuss some of the other parameters presented in Table III.

The calculated ϵ's for protons and α particles are 0.018 and 0.077, respectively. The latter is close to the values given in Table III. The value listed there for protons is much higher, and indicates that the first-order treatment of the recoil effect is not sufficient to explain the observed asymmetry in the proton angular distributions.

On the basis of a few tests, which showed that the fit results were rather insensitive for any value of k between 0.6 and 1.0, we have set the anisotropy parameter for the final fits k to unity, corresponding to an isotropic c.m. distribution for evaporated particles.

In Fig. 8 the values of σ_{ER} found at 12.4 and 19.7 MeV/nucleon are compared to the values from the

TABLE III. Parameters describing the angular distributions of LP's measured in coincidence with ER's having $Z_{ER} \geq 15$ for the $^{28}Si + ^{28}Si$ reaction at 12.4, 19.7, and 30.0 MeV/nucleon. Multiplicities for evaporated particles M_E, for pre-equilibrium particle distribution in particles M_{PE}, and their sum M are derived via an integration of the LP distributions that were normalized to the corresponding inclusive ER cross sections.

Particle		p	p	p	α	α	α
Beam energy	[MeV/n]	12.4	19.7	30.0	12.4	19.7	30.0
χ^2 per degree of freedom		77.7	2.31	3.17	19.9	1.73	1.19
θ_{HI}	[degrees]	5	4	4.5	5	4	4.5
ϵ		0.067(1)	0.096(6)	0.038(7)	0.079(3)	0.084(2)	0.073(5)
σ_{ER}	[c]	0.0147	0.018(1)	0.018	0.0071(1)	0.0097(1)	0.0097
k		1.0	1.0	1.0	1.0	1.0	1.0
T	[MeV]	4.65(4)	6.3(2)	6.9(2)	6.79(6)	9.5(1)	12.3(2)
T_C	[MeV]	0.94(3)	0.68(5)	0.68	0.84(3)	1.59(5)	1.59
E_C	[MeV]	1.39(2)	2.27(6)	2.27	6.6(1)	6.5(1)	6.5
N_E		4.32(2) 10^3	8.7(4) 10^5	2.58(9) 10^4	1.25(4) 10^4	1.43(2) 10^6	2.46(6) 10^4
μ		0.037	0.037	0.037	0.166	0.166	0.166
ν		0.491	0.491	0.491	0.461	0.461	0.461
$\sigma_\parallel$	[c]	0.076(2)	0.086(2)	0.127(5)	0.0258(4)	0.0385(8)	0.045(2)
$\sigma_\perp$	[c]	0.054(1)	0.122(3)	0.119(4)	0.0380(4)	0.0640(8)	0.064(4)
N_{PE}		5.71(1) 10^2	4.7(6) 10^4	9.0(5) 10^2	1.98(8) 10^4	1.29(5) 10^5	3.7(3) 10^3
M_E		3.9(6)	2.2(3)	2.0(3)	2.1(3)	1.1(2)	0.76(10)
M_{PE}		0.7(1)	0.58(9)	0.45(7)	0.56(8)	0.30(5)	0.31(5)
M		4.6(7)	2.8(4)	2.5(4)	2.6(4)	1.4(2)	1.1(2)

analysis of the inclusive ER spectra (Sec. III) and to the results of our Monte Carlo model (Sec. IV). The comparison shows that our fits to the LP spectra yield realistic values for σ_{ER}. The value of σ_{ER} for protons (solid arrow) corresponds to the coincident ER's with the lowest Z_{ER}, the one for α particles (dashed arrow) to ER's with the highest Z_{ER}. This may indicate that α particles are emitted preferably in the beginning of the decay chain.

A realistic result is also obtained at 12.4 and 19.7 MeV/nucleon for E_C. These values are close to the values for the Coulomb potential V_C calculated by $V_C = 1.44 Z_{ER} Z_{LP} / (1.2 A_{ER}^{1/3} + 1.2 A_{LP}^{1/3})$. To reduce the number of free parameters at 30.0 MeV/nucleon E_C and T_C were fixed to their value at 19.7 MeV/nucleon. The values of T_C are comparable as those listed in Ref. [22].

The measured spectra are well described by the analytical model. An example is given in Figs. 9–12 for the 19.7 MeV/nucleon data. A deviation is present in the description of two α spectra measured in the 12.4 MeV/nucleon reaction at $\theta_L = 15°$, $\phi_L = 0°$ and $\theta_L = 24°$, $\phi_L = 0°$ for energies above 60 MeV. The excess in the LP data is caused by α particles emitted in coincidence with a projectilelike fragment, which could not be excluded from the α-ER coincidences at small LP angles due to the insufficient element resolution of the HI detector. An experimental excess in the form of a high-energy tail is also observed in the 30.0 MeV/nucleon proton spectra at $\theta_L = 15°$, $\phi_L = 0°$ and $\theta_L = 15°$, $\phi_L = 180°$. Due to the small cross section of this extra yield, its contribution to the overall proton multiplicity is below the 1% level and will, within the present accuracy, not influence the results that are based on this quantity.

With the parameters listed in Table III and Eqs. (2), (9), and (14) we can separate the angular distributions into contributions of equilibrium and pre-equilibrium particles. For all angular distributions, the yield of evaporated particles dominates the angular range between 45° and 60°, whereas the pre-equilibrium yield dominates at backward angles. The existence of angles where one of the components dominates, along with the required fore-aft symmetry, makes the decomposition unambiguous.

C. Invariant-velocity distributions

The proton and α-particle invariant-velocity distributions shown in Fig. 13 are made using Eqs. (2), (9), and (14), which describe the LP yield at 19.7 MeV/nucleon with the parameters given in Table III. The invariant-velocity spectra at 12.4 and 30.0 MeV/nucleon have similar features.

In the velocity spectra the influence of the coincidence requirement is visible as an extra yield on the left-hand side of the picture and below the velocities of the sources (the ER detector was placed on the right-hand side). The pre-equilibrium α particles are clearly emitted from two separate sources, one at projectile and one at target velocity. The two Gaussians, by which the pre-equilibrium proton distributions are described, have such an overlap that they form an anisotropic elongated distribution with its center at $v_{c.m.}$. Such a source at c.m. velocity of pre-

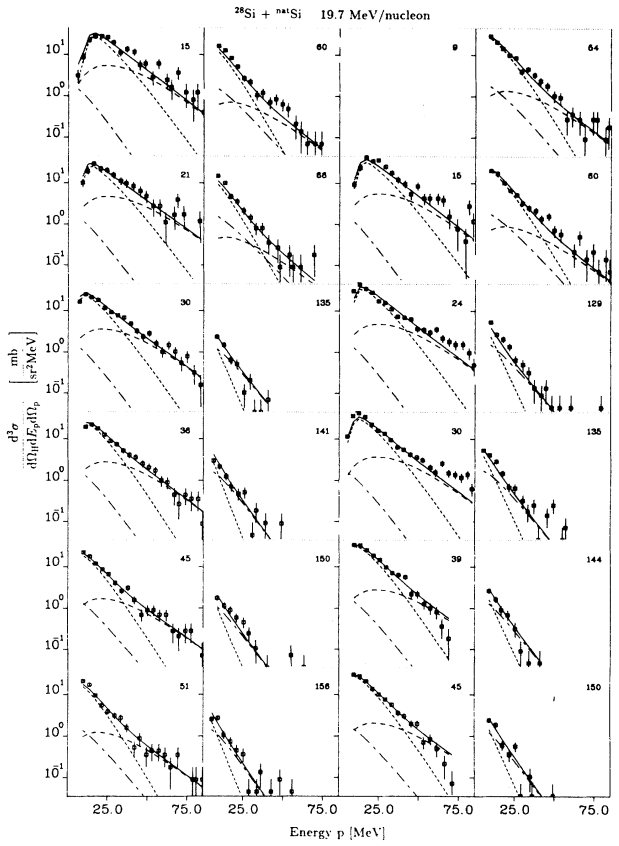

FIG. 9. In-plane angular distribution for protons emitted in coincidence with ER's with $Z_{ER} \geq 15$ at 4° in the 19.7 MeV/nucleon ^{28}Si+^{28}Si reaction. The angle θ_L is shown in each spectrum. For the first two columns $\phi_L = 0°$, whereas for the last two columns $\phi_L = 180°$. The evaporation yield is given by the short-dashed line, the projectile pre-equilibrium yield by the long-dashed line, and the target pre-equilibrium yield by the dash-dotted line. The solid line gives the total yield.

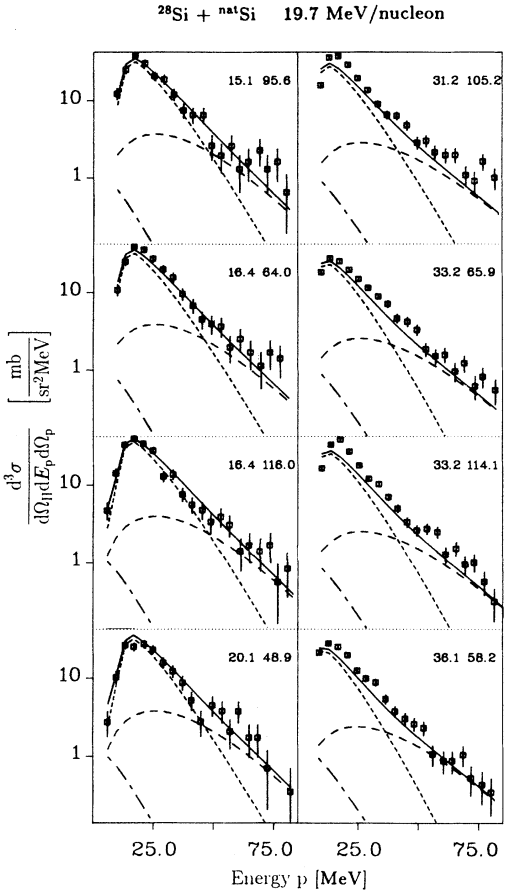

FIG. 10. Out-of-plane angular distribution for protons emitted in coincidence with ER's with $Z_{ER} \geq 15$ at 4° in the 19.7 MeV/nucleon ^{28}Si+^{28}Si reaction. The angles θ_L and ϕ_L are shown in each spectrum.

equilibrium neutrons was found in the reaction ^{40}Ar+^{40}Ca at 20 MeV/nucleon [24]. Sources of pre-equilibrium nucleons with c.m. velocity at half the beam velocity are described by a microscopic quantum-mechanical model that shows that these nucleons are pre-equilibrium particles emitted after zero (Fermi jets), one, or more collisions with other nucleons [24–26].

D. Momentum widths of pre-equilibrium particles

In the Friedman model [27] for the parallel momentum width $\sigma_\parallel$, the detected particle is the only part of the projectile that is not absorbed by the target. If one uses an approximate wave function that describes the relative separation between the fragment and the remaining part of the projectile, the model gives the parallel momentum distribution of the fragment. For the detected projectile fragment F with mass m_F and mass number A_F the $\sigma_\parallel$ is given by

$$\sigma_\parallel^2 = \frac{\hbar\mu}{2x_0}\left[\frac{1+y/2}{\sqrt{1+y}} + \frac{\hbar}{\mu x_0}\right]\sqrt{1-V_C/E_{\text{proj}}}\,. \quad (15)$$

One may write $\mu = \sqrt{2m_R E_s}$, $m_R = (m_R m_F)/(m_R + m_F)$, $x_0 = 1.2A_F^{1/3}$, and $y = Z_R Z_F e^2/(x_0 E_s)$ with Z_R and m_R the charge number and mass of the absorbed projectile residue R, respectively. E_s falls between the separation energy of the projectile into R and F and the energy needed to separate F when it is excited to just below its threshold for particle decay. The radius of the fragment is given by x_0 and the Coulomb energy between projectile and target is given by V_C. The model has been applied successfully to describe the properties of the projectilelike fragments [27,28].

The experimental values for $\sigma_\parallel$ and $\sigma_\perp$ as well as the results of calculations with Friedman's model [27] for absorptive breakup and Möring's Fermi-jet model [29] are listed in Table IV. For the α particles the agreement between Friedmans theory and experiment is within 30%. The calculated values for the proton widths are much higher than the values found experimentally. Although the Friedman model is less apt for protons than for α

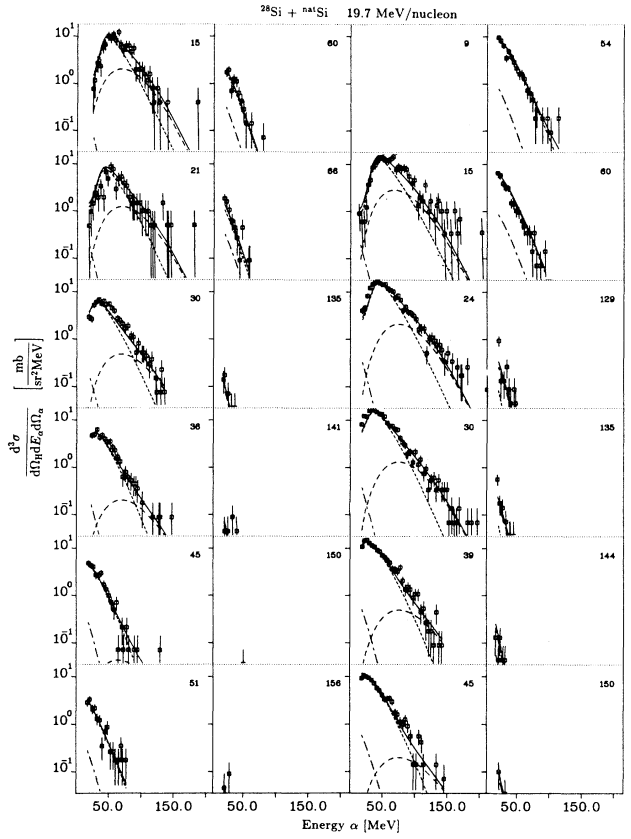

FIG. 11. In-plane angular distribution for α particles emitted in coincidence with ER's with $Z_{ER} \geq 15$ at 4° in the 19.7 MeV/nucleon ^{28}Si+^{28}Si reaction.

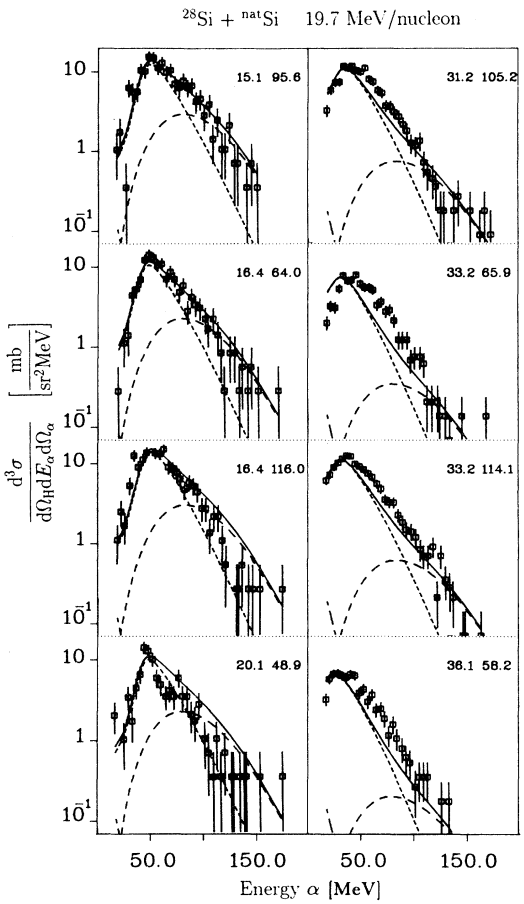

FIG. 12. Out-of-plane angular distribution for α particles emitted in coincidence with ER's with $Z_{ER} \geq 15$ at 4° in the 19.7 MeV/nucleon ^{28}Si+^{28}Si reaction.

particles, this result indicates that the protons might be produced via other mechanisms, which is consistent with the observations made in Sec. IV C that the pre-equilibrium protons are emitted by jetting processes and after collisions with other nucleons. The Fermi-jet model of Ref. [29] is only able to calculate the momentum widths for protons and α particles. It yields values too low for $\sigma_{\parallel}$ and $\sigma_{\perp}$ for all beam energies. Since this pure mean-field model does not include the broadening due to two-body interactions, the calculated values should be regarded as a lower limit [1].

The momentum σ_0, which has a meaning in Goldhaber's breakup model [30], is calculated from the $\sigma_{\parallel}$ and listed in Table IV. The σ_0 from the ^{28}Si+^{28}Si experiments fit into the systematics [27,31], which, in contrast to the basic assumption of the Goldhaber model, depend on the beam energy.

E. Multiplicities

Although the detectors in the three experiments cover only a limited part of the total solid angle, our fit to the coincident LP yield allows us to integrate the LP yield over the LP angle and energy. The resulting value, normalized to the inclusive ER cross section for the same gate on v_{ER} and Z_{ER}, is equal to the average number of LP's emitted per ER (i.e., the LP multiplicity). As long as the fit to the data is reasonable, regardless of the assumptions of that fit, the integrated LP yield deduced from the fit is model independent; even a polynomial will do [32]. As we showed in Ref. [6] one can determine with reasonable accuracy (10%) the multiplicity of LP's using this method. For each set of fitted parameters, characterized by a χ^2 value smaller than 3.5, the total extracted multiplicities differ by at most 10%.

Table III and Fig. 14 give the multiplicities M_E and M_{PE} of the evaporated and the pre-equilibrium LP's that were coincident with $Z_{ER} \geq 15$ for the three beam energies. Only the values for protons and α particles are listed, since they comprise more than 90% of the total charged particle yield. M_E and M_{PE} are the largest at 12.4 MeV/nucleon, and decrease with increasing beam energy. The values for the total multiplicity M are roughly a factor of 2 higher in the 12.4 MeV/nucleon experiment than in the 19.7 and 30.0 MeV/nucleon experiments. Since M at 19.7 and 30.0 MeV/nucleon is determined only for $Z_{ER} \geq 15$, which selects only a half of all ER's to be roughly twice as large and therefore at most

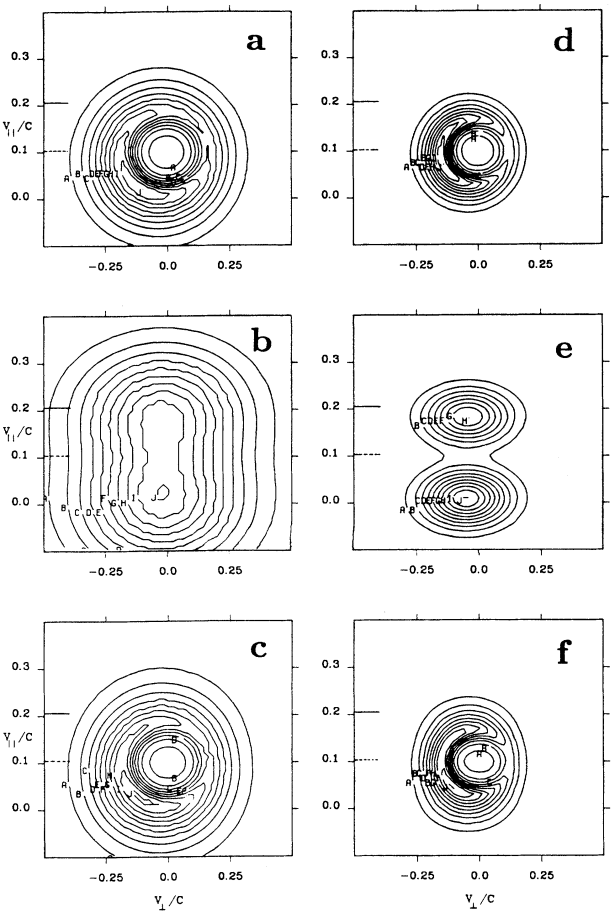

FIG. 13. Invariant-velocity distribution in the laboratory frame for protons and α particles produced in the reaction $^{28}Si+^{28}Si$ at 19.7 MeV/nucleon calculated from a fit to the data. (a) Proton evaporation component, (b) proton pre-equilibrium component, (c) sum of the evaporation and the pre-equilibrium components, (d), (e), and (f) the same for α particles. The magnitude of the beam and c.m. velocity are given by the solid and dashed lines, respectively. The invariant-velocity distribution at 12.4 and 30.0 MeV/nucleon have similar characteristics to those pictured here.

equal to those at 12.4 MeV/nucleon. Considering that the maximum excitation energy of fully fused systems differs greatly between 12.4 and 30.0 MeV/nucleon, the result comes as a surprise. However, the results presented later on offer a plausible explanation.

F. Initial properties of compound nuclei

In Ref. [6] we have shown that the average initial properties of the CN can be accurately reconstructed. We now apply the method to the case of excited nuclei produced in incomplete fusion reactions. The average charge $\overline{Z}_{\rm CN}$, mass number $\overline{A}_{\rm CN}$, and excitation energy $\overline{E}^{\,*}_{\rm CN}$ of the CN can be calculated via

$$\overline{Z}_{\rm CN}=\sum_{i=p,\alpha} Z(i)M_E(i)+\overline{Z}_{\rm ER}\ , \tag{16}$$

$$\overline{A}_{\rm CN}=2\overline{Z}_{\rm CN}\ , \tag{17}$$

$$\overline{E}^{\,*}_{\rm CN}=\sum_{i=p,n,\alpha}[\overline{E}_E(i)+m(i)c^2]M_E(i) +m_{\overline{\rm ER}}c^2-m_{\rm CN}c^2\ , \tag{18}$$

in which the average c.m. kinetic energy and multiplicity of the evaporated LP's of type i are represented by $\overline{E}_E(i)$ and $M_E(i)$, respectively, and the average charge number of the ER is given by $\overline{Z}_{\rm ER}$. As in all following calculations, we have assumed that the neutron multiplicity equals the proton multiplicity as it must, because all decay products are near the line $A=2Z$. The quantity $m_{\overline{\rm ER}}$ is the mass of the nucleus with mass and charge number $\overline{A}_{\rm ER}=2\overline{Z}_{\rm ER},\overline{Z}_{\rm ER}$.

The proton and α-particle multiplicities were taken from Table III. To first order, the neglect of the mass and energy carried off by other H and He isotopes (less then 10% of the proton plus α-particle yield) do not

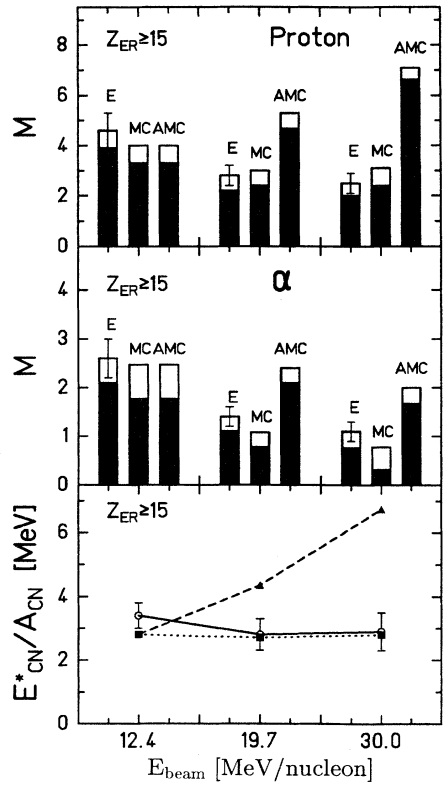

FIG. 14. Multiplicities of protons and α particles, that are emitted in coincidence with an ER with $Z_{\rm ER}\geq 15$ as a function of beam energy for the $^{28}Si+^{28}Si$ reaction are shown in the two upper parts of the figure. The lower part of the figure shows the corresponding $E^*_{\rm CN}$ distribution. The black area gives the contribution of evaporated particles, the blank area that of the pre-equilibrium particles. The labels E and open points represent experimental results, the labels MC and squares are from the Monte Carlo model discussed in Sec. V, the labels AMC and triangles are from the alternative Monte Carlo model also discussed in Sec. V.

TABLE IV. Experimental and calculated momentum widths for the pre-equilibrium particle distribution in ^{28}Si+^{28}Si reactions at 12.4, 19.7, and 30.0 MeV/nucleon. σ_0 is calculated from the data using the Goldhaber model.

Widths (MeV/c) \ Particle, Beam energy (MeVn)	p 12.4	p 19.7	p 30.0	α 12.4	α 19.7	α 30.0
		Experiment				
$\sigma_\parallel$	71(2)	80(2)	119(5)	96(2)	144(3)	164(2)
$\sigma_\perp$	51(1)	115(2)	111(4)	142(2)	238(3)	237(8)
		Friedman				
$\sigma_\parallel$	154	156	159	135	137	139
		Möring				
$\sigma_\parallel$	41	41	41			
$\sigma_\perp$	41	41	41			
		Goldhaber				
σ_0	71(2)	80(2)	119(5)	51(1)	76(2)	87(2)

affect the extracted excitation energy per nucleon. The average LP kinetic energy $\bar{E}_E(i)$ was calculated by averaging the LP kinetic energy over the c.m. energy distribution of evaporated particles, Eq. (1). For neutrons we have applied the same procedure using the proton parameters listed in Table III with the Coulomb barrier turned off (i.e., $E_C=0$ MeV). The results of these calculations are presented in Table VI, together with results of the Monte Carlo calculations (see Sec. V).

From this table we see that the average charge and mass numbers and the average excitation energy per nucleon of the CN at 19.7 and 30.0 MeV/nucleon are nearly equal. However, the excitation energies at the two highest beam energies are determined only for CN's that decayed to ER's with $Z_{ER} \geq 15$, and these contribute to only half of the total ER yield. Therefore, this experimentally determined average excitation energy of CN's should be corrected for the yield of ER's with $Z_{ER} < 15$. The evaporation of 4–8 nucleons or 1–2 α particles more corresponds to 30–60 MeV or 0.7–1.5 MeV/nucleon more excitation energy. This indicates that the average excitation energy of CN's decaying to ER's at 12.4, 19.7, and 30.0 MeV/nucleon remains rather constant at the level of 3.7–4.5 MeV/nucleon, although much more excitation energy is available at the two highest beam energies. This may be interpreted as a signature of a limitation of the excitation energy of CN's that decay to ER's, which is discussed in more detail in Sec. V.

G. The level density parameter

In Sec. IV F we have calculated the average CN excitation energy. If we know the level density parameter a then we can calculate the initial temperature T of the CN via [34]

$$T=\left[\frac{E^*_{CN}}{a}\right]^{1/2}. \tag{19}$$

At excitation energies below 0.5 MeV/nucleon the value of a is well known. It is nearly proportional to the mass number of the nucleus, $w=A_{CN}/a$ increases only slightly for heavier nuclei [34]. References [35,36] stated that for a neutron cascade the slope parameter T is close to the initial CN temperature provided that the shape of the c.m. neutron spectrum is described by $E^{0.45}_{c.m.}\exp(-E_{c.m.}/T)$. Fits of Eq. (1) multiplied with the Jacobian $\sqrt{E_L/E_{c.m.}}$ (E_L is the laboratory energy of the LP) to the proton laboratory spectra generated by the statistical model PACE2 [37] show that T for protons is within 0.5 MeV equal to the initial temperature of the nucleus before its decay and that T is nearly independent of the critical angular momentum l_{crit} of the triangular spin distribution used in the model.

The identification of the spectrum slope parameter for protons as the initial temperature of the CN is more problematic if the protons are evaporated from CN's that are formed in an incomplete fusion reaction. In that case the velocity of the evaporation source is distributed around the c.m. velocity, and this results in an somewhat larger T. Since the widths of the ER velocity distribution are measured, one can unfold the LP spectra a correction for this broadening. The recoil corrections are negligible at 12.4 MeV/nucleon and would be at the most -10% at 30.0 MeV/nucleon [38]. However, the results of our Monte Carlo calculation (see the next section) presented in Fig. 15 shows that incomplete fusion also causes a broad distribution in the excitation energy per nucleon at 19.7 and 30.0 MeV/nucleon, making the interpretation of the proton slope parameter as the initial temperature impossible. Only the E^*_{CN}/A_{CN} distribution at 12.4 MeV/nucleon has a small enough width *a eqn: syntax error file /usr/tmp/Pgb7200, between lines 760 and 760* to interpret the proton slope parameter as the average initial CN temperature. Using the result $E^*_{CN}/A_{CN}=3.4(4)$ MeV from Table VI and the value $T=4.65(50)$ taken from Table III (the error is estimated in this section) we find that at 12.4 MeV/nucleon $w=6.4(15)$ MeV. This

value is consistent with the widely used value of $w=8$ MeV [1]. These results indicate that the picture of the fusion process at 12.4 MeV/nucleon is completely connected with the systematics at lower energies.

Because α particle are emitted preferentially from high-spin states and have to overcome a larger angular momentum barrier than protons, the T of α particles is larger than for protons (see Table III). Moreover, the corrections due to motion of the hot nucleus (from incomplete fusion and initial evaporations) are larger in this case than for protons and will further increase the observed T. Hence, quantitative extractions of w from the αT parameters are not possible.

H. Charge and energy balance

In the previous sections we have seen that the CN formed at 12.4 MeV/nucleon contains nearly all of the 56 nucleons that are available in the reaction, while at 19.7 and 30.0 MeV/nucleon the CN that decayed to ER's with $Z_{\mathrm{ER}} \geq 15$ contained 40–42 nucleons. We have calculated the average charge that is emitted in LP's and ER's via

$$\bar{Z}_{\mathrm{tot}} = \sum_{i=p,\alpha} Z(i)[M_E(i)+M_{\mathrm{PE}}(i)]+\bar{Z}_{\mathrm{ER}} \ . \tag{20}$$

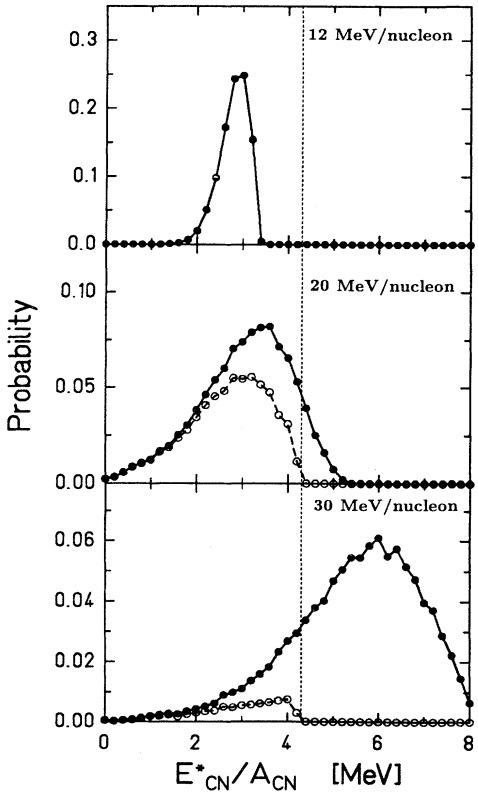

FIG. 15. CN excitation energy distributions calculated by the Monte Carlo model described in this paper for the ^{28}Si+^{28}Si reactions at 12.4, 19.7, and 30.0 MeV/nucleon. The closed points reflect the probability for which a CN is formed with a given $E^*_{\mathrm{CN}}/A_{\mathrm{CN}}$ under the assumption of the emission of a targetlike and projectilelike fragment. The open points shows the number of events for which $E^*_{\mathrm{CN}}/A_{\mathrm{CN}} \leq E^*_{\mathrm{lim}}/A = 4.3$ MeV and $Z_{\mathrm{ER}} \geq 15$.

The results are shown in Fig. 16. In the reaction at 12.4 MeV/nucleon there is no missing charge, which shows that we were able to detect all of the charged particles that are emitted in processes in which ER's are produced.

At 19.7 and 30.0 MeV/nucleon about 7–8 charge units are missing, corresponding to 14–16 nucleons. The average missing energy $\overline{\Delta E}$, the energy (kinetic energy plus rest mass) of the missing particles, is given by

$$\begin{aligned}\overline{\Delta E} = {} & m_P c^2 + E_P + m_T c^2 + E_T \\ & - \sum_{i=p,n,\alpha} [\bar{E}_E(i)+m(i)c^2]M_E(i) \\ & - \sum_{i=p,n,\alpha} [\bar{E}_{\mathrm{PE}}(i)+m(i)c^2]M_{\mathrm{PE}}(i) - m_{\overline{\mathrm{ER}}}c^2 \end{aligned} \tag{21}$$

with E_P, m_P and E_T, m_T the c.m. kinetic energy and mass of the projectile and target, respectively. The average kinetic energy of the pre-equilibrium particles $\bar{E}_{\mathrm{PE}}(i)$ is calculated from the velocity distributions of projectile [Eq. (8)] and target pre-equilibrium particles. The parameters used in these calculations were taken from Table III. In the calculation of $\bar{E}_E(n)$, the neutron parameters were taken to be identical to the proton parameters, except that the neutron Coulomb energy was set to $E_C=0$ MeV. Under the further assumption that the energy of the emitted γ rays and the average recoil energy of the ER is about 10 MeV [6], the average kinetic energy $\bar{E}$ of the missing nucleons is calculated from $\overline{\Delta E}$ and shown in Table V for three cases: (1) all of the missing nucleons are bound into one or (2) two fragments, and (3) the missing nucleons are unbound.

At 12.4 MeV/nucleon the average kinetic energy of the missing nucleons is zero within the zero error bars. This result is consistent with the zero missing charge at this beam energy and gives confidence in the results obtained for the experiments at the other beam energies. At 19.7 and 30.0 MeV/nucleon the kinetic energy of the missing nucleons can be quite high. In Table V we have listed the velocities to which these kinetic energies correspond. If the missing nucleons are not bound, their velocities will

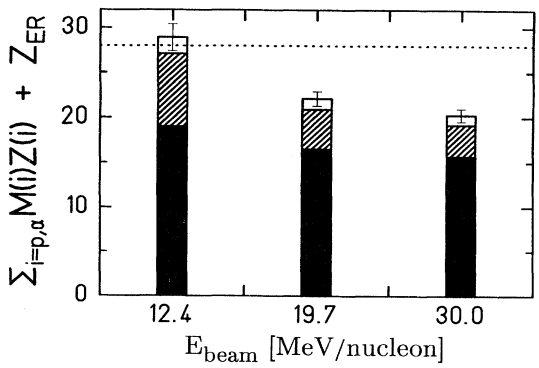

FIG. 16. Average charge balance for the ^{28}Si+^{28}Si reactions at 12.4, 19.7, and 30.0 MeV/nucleon. The black area gives the average charge number of the ER, the hatched and blank areas give the average number of charges emitted per ER for evaporated and pre-equilibrium particles, respectively.

TABLE V. Average kinetic energies $\bar{E}$ and velocities v of the missing nucleons at 12.4, 19.7, and 30.0 MeV/nucleon. $\bar{E}$ and v are calculated assuming that (1) all nucleons are unbound, (2) all missing nucleons are bound in two equal fragments, and (3) all the missing nucleons are bound in a single fragment. Errors in $\bar{E}$ are estimated to be in the order of 40 MeV. From the kinetic energy the c.m. velocity of the missing particles v is calculated for both cases. v_P is the c.m. velocity of the projectile.

Beam energy	(MeV/nucleon)	12.4	19.7	30.0
$\bar{E}$ (1)	(MeV)	−6	28	144
$\bar{E}$ (2)	(MeV)	−26	86	220
$\bar{E}$ (3)	(MeV)	−25	98	248
v (1)	(cm/ns)		2(2)	4.5(7)
v (2)	(cm/ns)		4.1(7)	5.5(6)
v (3)	(cm/ns)		4.2(9)	5.9(7)
v_P	(cm/ns)	2.4	3.1	3.8

be such that they should contribute to our observed LP yields at forward angles and backward angles. However, any measured surplus of nucleons is already incorporated in the charge and energy balance. Therefore, at 19.7 and 30.0 MeV/nucleon both the missing mass and missing energy must be taken away by one or more composite particle(s) ($Z \geq 3$). The Gaussian shape of the invariant ER velocity distribution with a center at $\mathbf{v}_{\text{c.m.}}$ excludes the possibility that all the nucleons are emitted in a single fragment, since that would cause a central dip in the ER velocity distributions (see also Sec. V). More than two fragments are also unlikely because this would imply that the average charge of the fragments would be close to two and would therefore contribute to our observed yields. Hence we deduce that two particles with $A=6-8$ are emitted in the early stages of the collision with velocities above that of the projectile or target in the c.m. system. Since a high multiplicity (about 1) of $A=6-8$ fragments that are coincident with ER's is not observed by the multidetector system, these particles must be emitted at small forward ($<15°$) and at large backward angles ($>150°$).

The following picture of the fusion process emerges: at 12.4 MeV/nucleon the two Si nuclei fuse almost completely, only a few nucleons are emitted before equilibrium is reached. In addition to the observed preequilibrium LP emission, at 19.7 and 30.0 MeV/nucleon two fragments with $A=6-8$ are emitted in opposite directions. Their average velocities, which are close to the target and projectile velocity, and their multiplicities, which are about unity for the reaction channels studied, are similar to those observed for projectilelike and targetlike fragments produced in peripheral reactions. This suggests that the reactions in which the fragments and the CN are produced are mutual breakup-fusion reactions in which both the projectile and the target nucleus undergo the breakup process.

In Sec. IV F we remarked that CN's formed at 19.7 and 30.0 MeV/nucleon have a much lower excitation energy than the total available c.m. energy. The missing nucleons, bound into fragments, are quite energetic, and therefore this low excitation energy might have a simple explanation. However, the velocity distributions of projectile and target fragments in breakup reactions have approximately a Gaussian form with the most probable fragment velocities at the velocities of the projectile and target nucleus. Therefore, regardless of the mass of the breakup fragments, the energy per nucleon of the CN formed should simply be the same as for fully fused nuclei if binding energy effects are neglected, about 5 and 7.5 MeV/nucleon at 19.7 and 30.0 MeV/nucleon, respectively. The results from Sec. IV F indicate that almost all CN's decaying by LP evaporation had excitation energies well below these values. The energy balance then implies that the fragments, which were produced in reactions in which ER's were produced too, should have velocities that exceed those of the projectile or target nuclei. Thus ER's are formed only when the fusion dynamics is such that the CN will have $E^*_{\text{CN}}/A_{\text{CN}}$ lower than a certain maximum value, the limiting excitation energy per nucleon, E^*_{lim}/A.

In such a picture the low ER cross section at 30 MeV/nucleon can be explained. In order to create a CN with excitation energy below E^*_{lim}/A, at least one of the fragment velocities must be much higher than the projectile or target velocity. This velocity lies in the tails of the Gaussian fragment velocity distribution. Consequently, CN's with energies below E^*_{lim}/A have a low production probability. In Ref. [33] we have demonstrated this effect in a more qualitative manner by a schematic Monte Carlo program that simulated the effects of the incomplete fusion process on the properties of the CN and we deduced from the results that $E^*_{\text{lim}}/A=4.6(5)$ MeV.

V. MONTE CARLO CALCULATIONS

A. Description

To check the conclusion from Sec. IV we made a Monte Carlo model of the fusion process, which allowed us to calculate observables that can be compared to the experimental ones.

In the Monte Carlo model the formation and decay of the CN's is calculated in several steps.

(1) At 19.7 and 30.0 MeV/nucleon (not at 12.4 MeV/nucleon) two fragments are created in the breakup of the projectile and target nucleus. The fragment velocities are chosen such that their velocity distributions have Gaussian shapes, which are centered at the target and projectile velocities. The widths of the velocity distributions are derived from the momentum width $\sigma_{\parallel}$, which

we calculated from Goldhaber's model [30] using the σ_0 of α particles listed in Table IV. The parallel velocity width is calculated directly from the model, while the perpendicular width was chosen to be proportional to the parallel velocity, with the proportionality constant $\sigma_\perp/\sigma_\parallel$ independent of the mass of the fragments. As a first guess we have set $\sigma_\perp/\sigma_\parallel=1$. The mass numbers of the fragments are chosen in such a way that the distribution of the mass number has a Gaussian form. The centroid of this distribution $A_{\rm cen}$ was taken to be equal to half of the measured missing mass (in mass units). The width of the mass distributions $\sigma_{A_{\rm cen}}$ (in mass units) satisfies the prescription that particles that could be measured in the experiment, e.g., H and He isotopes and heavy ions with $M>8$, and thus could not contribute to the missing charge, should be seldom produced. This implies a rather low value of $\sigma_{A_{\rm cen}}=2-3$.

(2) At all beam energies the emission of pre-equilibrium protons and α particles is simulated. The emission probability is such that the average multiplicity of these particles is the same as found in the experiment for pre-equilibrium particles coincident with ER's ($Z_{\rm ER}\geq 15$) and which are listed in Table III. The velocities of the pre-equilibrium particles from the projectile source are chosen in such a way that their c.m. velocity distribution is given by Eq. (8), with the parameters given in Table III. The emission of LP's from the target is simulated in a similar way.

(3) Then we assume that the remaining parts of the target and projectile nuclei fuse to form a CN. The initial properties of the CN are calculated using the conservation laws for baryon number, charge, momentum, and energy.

(4) In the next step the decay of the CN by LP evaporation is simulated. In order to avoid the complications in the description of the evaporation process of highly excited nuclei (see, e.g., Ref. [39]) we have used Eq. (1) together with the parameters listed in Table III as basis for the computation of the branching ratios and of the energies of the evaporated particles. At each decay step the chance of evaporating a proton, neutron, or α particle is proportional to the corresponding multiplicity (the multiplicity of neutrons is assumed to be equal to that of protons). Note that the rather successful analytical statistical model of the authors of Ref. [40] is solely based on an identical determination of the branching ratios. The emission angles are chosen such that the LP's are emitted isotropically, which is consistent with $k=1$ in Table III. The probability of evaporating a particle with a given c.m. energy is proportional to the cross section for that energy in the c.m. system. From this the c.m. velocity of the particle and the velocity of the daugher nucleus is calculated, using momentum conservation. The excitation energy of the daughter nucleus is then the difference of the total kinetic energies before and after the evaporation plus the Q value. A decay is prohibited if any of the conservation laws is violated. The cascade is stopped once these laws forbid the emission of particles.

In the last step (5) the various spectra are updated with optional conditions such as an upper limit on $E^*_{\rm CN}/A_{\rm CN}$, which simulates the effect of $E^*_{\rm lim}/A$, or the lower limit $Z_{\rm ER}I<15$, which simulates the experimental cuts on the charge of the ER.

An inaccuracy of this method to simulate the decay of a CN is that the multiplicities and the LP distributions are determined for $Z_{\rm ER}\geq 15$ and are therefore less suited to describe decay chains in which ER's with $Z_{\rm ER}<15$ are produced. For that reason we have derived the normalization constant for Monte Carlo calculations from the number of ER's with $Z_{\rm ER}\geq 15$ generated in the calculations and the experimental cross section for ER's with $Z_{\rm ER}\geq 15$.

We have also performed calculations in which only a single target or projectilelike fragment, containing on average all the missing nucleons, is emitted during the fusion process. The results, most noticeably the volcano shape of the ER velocity distribution, clearly show that such a scenario is not consistent with the available data. The authors of Ref. [24] concluded for the nearly symmetric reaction ^{40}Ar+^{40}Ca at 20.0 MeV/nucleon that CN's are formed in fusion reactions in which a few pre-equilibrium particles are emitted, but no fragments. Their analytical model for the ER mass and charge distribution did not consider $E^*_{\rm lim}/A$. This scenario of the incomplete fusion process is similar to the one we use for the 12.4 MeV/nucleon ^{28}Si+^{28}Si reactions. To compare such a scenario with the data we have made an alternative Monte Carlo model which omits the emission of the projectilelike and targetlike fragments at 19.7 and 30.0 MeV/nucleon. The collision dynamics at these energies in the alternative Monte Carlo model is therefore the same as at 12.4 MeV/nucleon. Furthermore, we have set $E^*_{\rm lim}/A=100$ MeV to remove any influence of $E^*_{\rm lim}/A$ on the results.

B. Results

The Monte Carlo code allows us to check the consistency of our scenario of the fusion process with the measured spectra and other observables. Furthermore, it allows us to determine $E^*_{\rm lim}/A$, the width of the fragment mass distribution $\sigma_{A_{\rm cen}}$ and the ratio $\sigma_\perp/\sigma_\parallel$, which we could not determine *a priori*. In Table VI the values of these parameters, for which the calculations best reproduce the experimental data, are listed.

In Fig. 15 the calculated full distributions of $E^*_{\rm CN}/A_{\rm CN}$ are shown together with the distribution of $E^*_{\rm CN}/A_{\rm CN}$ limited by $E^*_{\rm lim}/A=4.3$ MeV and $Z_{\rm ER}\geq 15$. The effect of $E^*_{\rm lim}/A$ at 12.4 and 19.7 MeV/nucleon is rather small compared to the effects at 30.0 MeV/nucleon. At that beam energy the presence of $E^*_{\rm lim}/A$ has a direct influence on the average $E^*_{\rm CN}/A_{\rm CN}$ of reactions in which ER's with $Z_{\rm ER}\geq 15$ are formed, and on their cross section. The experimental value for $E^*_{\rm CN}/A_{\rm CN}$ (see Table VI) at 30 MeV/nucleon cannot be reproduced without the assumption of a limiting excitation energy.

From the parameters that govern the properties of the fragments only the ratio $\sigma_\perp/\sigma_\parallel$ is significantly changed from its initial (guessed) value $\sigma_\perp/\sigma_\parallel=1$. The calcula-

tions show that this parameter has a limited influence on the ER angular distribution and on the excitation energy of the CN. Generally, a change of the fragment velocity widths does not have a large effect on the calculated angular distributions of ER's. If the widths increase then the average excitation energy of the CN is decreased (the CN has on average a larger c.m. kinetic energy) and consequently the recoils imparted to the ER by the evaporated particles are reduced. A similar argument explains the observation that a change in the widths of the fragment mass distributions has also a small effect on the widths of the ER distribution.

The calculations also demonstrate that the experimental setup employed could not detect the fragments with $A=6-8$. The projectilelike fragments are predominantly emitted in a narrow cone ($\theta<5°$) around the beam axis in which none of our detectors was able to detect them properly, while the targetlike fragments have a velocity close to zero in the laboratory frame and are stopped in the ΔE detectors of the multidetector system.

Table VI shows that there is a rather good agreement of most of the experimental and calculated quantities describing the average properties of CN's. Figure 14 indicates that in the Monte Carlo model too few α particles and too many protons are evaporated at 30.0 MeV/nucleon. In the calculations the branching ratios were set proportional to the experimental multiplicities and are independent of the excitation energy of the evaporating nucleus. Clearly, this method works fine at 12.4 and 19.7 MeV/nucleon but is insufficient at 30.0 MeV/nucleon. The experiments show (see Figs. 6 and 14) that the charge and excitation energy distributions of the CN at 19.7 and 30.0 MeV/nucleon are almost equal. Therefore, the difference in the branching ratios indicates that there should be at least one other quantity, probably the average angular momentum, by which the CN's differ. The alternative Monte Carlo model overestimates the multiplicities of protons and α particles at 19.7 and 30.0 MeV/nucleon by a factor 2–3. Since the model neglects the effect of pre-equilibrium fragment emission as well as $E^*_{\rm lim}/A$, the $E^*_{\rm CN}/A_{\rm CN}$ is much higher, causing more particles to be evaporated. Note that the two models differ only at the highest two beam energies (see Sec. V A). Since the average $A_{\rm CN}$ is also higher in this alternative model, the $Z_{\rm ER}$ distribution calculated at 30.0 MeV/nucleon is not too far off from the experimental one; see Fig. 6. However, the Monte Carlo models also allow us to calculate ER angular distributions. In Fig. 5 they are compared with the experimental distributions. These comparisons work strongly in favor of our proposed Monte Carlo model. The parallel widths of the ER velocity distributions are shown in Fig. 8. Here the results of the two models are the same as 19.7 MeV/nucleon. The alternative model underestimates the widths at 30.0 MeV/nucleon more then the proposed one. These results clearly show that the fusion processes studied at the beam energies of 19.7 and 30.0 MeV/nucleon are far from being "complete."

TABLE VI. Experimental results deduced from the charge and energy balance compared with the Monte Carlo results. The input parameters of the Monte Carlo model are given at the end of the table. Pre-equilibrium fragments with $Z\geq 3$ are not emitted at 12.4 MeV/nucleon. $A_{\rm cen}$ is the average fragment mass number, $\sigma_{A_{\rm cen}}$ is the width of the fragment mass distribution, and $\bar{v}$ is the average fragment velocity. The experimental value of $\bar{v}$ is taken from Table V, case (2).

		Experiment			Monte Carlo		
Beam energy	(MeV/nucleon)	12.4	19.7	30.0	12.4	19.7	30.0
			Results for $Z_{\rm ER}\geq 15$				
$\bar{Z}_{\rm CN}$		27(2)	21(2)	19(2)	27	21	19
$\bar{A}_{\rm CN}$		54(4)	42(4)	38(4)	53	42	38
$\bar{E}^*_{\rm CN}$	(MeV)	185(20)	118(20)	112(20)	149	112	110
$\overline{E^*_{\rm CN}/A_{\rm CN}}$	(MeV)	3.4(4)	2.8(5)	2.9(6)	2.8	2.7	2.8
$\bar{Z}_{\rm ER}$		19	16.5	15.7	19.2	16.6	15.5
$\bar{v}$	(cm/ns)		4.1(9)	5.5(7)		3.42	4.6
			Parameters of the Monte Carlo model				
$E^*_{\rm lim}/A$	(MeV)				4.3	4.3	4.3
σ_0	(MeV/c)					76.0	86.0
$\sigma_\perp/\sigma_\parallel$						0.5	0.3
$A_{\rm cen}$						6.0	7.5
$\sigma_{A_{\rm cen}}$						2.0	2.0

In general, the largest deviations of the proposed Monte Carlo model occur for $Z_{ER} < 15$. The deviations reflect that the parameters, which describe the LP properties in the model, were derived from spectra of LP's, which were coincident with ER's having $Z_{ER} \geq 15$.

From Fig. 15 and Table VI we see that almost all events generated in the Monte Carlo calculations for the reactions at 12.4 and 19.7 MeV/nucleon have $E^*_{CN}/A_{CN} < E^*_{lim}/A$, and this result is therefore consistent with the experimental result that the ER cross sections at those beam energies is not suppressed. However, for only a small fraction f of the events at 30.0 MeV/nucleon E^*_{CN}/A_{CN} is below E^*_{lim}/A. From Fig. 15 it is also evident that f strongly depends on E^*_{lim}/A. The value $f=0.1$, obtained via an extrapolation of the experimental ER cross sections at lower energies, would correspond to $E^*_{lim}/A=4.0$ MeV in our Monte Carlo model, while for $E^*_{lim}/A=4.3$ MeV (corresponding to $f=0.17$) the best agreement of the model with all the other experimental results is obtained. In view of the general problems associated with extrapolations (e.g., in this case a smooth extrapolation neglects the fact that below 19.7 MeV/nucleon the fusion mechanism changes from a fusion reaction in which only a few pre-equilibrium LP's are emitted into a breakup-fusion reaction) the results are consistent.

The ability of the model to determine the value E^*_{lim}/A is strongly dependent on the implementation of the reaction dynamics, most noticeably on the description of the correlations between the two fragments and the description of the emission of pre-equilibrium LP's. The rather good agreement of the results calculated with the model, in which no correlations between the two fragments are assumed and in which pre-equilibrium LP's have no correlation with each other or with the fragments show that, if these correlations exist, then they do not influence the gross properties of the reaction dynamics.

VI. SUMMARY

Detailed inclusive heavy-ion distributions and exclusive light-particle heavy-ion distributions have been measured for the reactions $^{28}Si+^{28}Si$ at 12.4, 19.7, and 30.0 MeV/nucleon. The present work is focused on those reaction channels in which an ER is formed. The inclusive measurements show that the ER cross section at 30.0 MeV/nucleon is a factor of 10 lower than calculated via a smooth extrapolation of ER cross sections measured at lower energies. For light systems this has not been observed before. Analytical functions based on the coincidence moving source model give a good description of the exclusive LP distributions and separate the LP yield into a pre-equilibrium and an evaporation component. The invariant-velocity distributions of pre-equilibrium protons are typical for jetting processes, while these distributions of pre-equilibrium α particles are typical for breakup type of processes. The total LP multiplicities are the largest at 12.4 MeV/nucleon and decrease with beam energy. The mass and energy balance show that CN's that decay to ER's with $Z_{ER} \geq 15$ have an initial excitation energy that does not exceed 3 MeV/nucleon. This implies an average excitation energy of 3.7–4.5 MeV/nucleon for all CN's decaying into ER's. The balances also indicate that at 19.7 and 30.0 MeV/nucleon for the reactions leading to ER's, a projectile and a target fragment with $A=6-8$ are emitted with an average c.m. velocity that exceeds that of the projectile and target nucleus. The results are consistent with a limiting excitation energy for nuclei, above which the nuclei decay mainly via other mechanisms and do not form ER's. A Monte Carlo simulation of the fusion process, based on these results, reproduces the experimental observables such as the coincident LP multiplicities, the ER angular distribution, and the Z_{ER} distribution assuming $E^*_{lim}/A=4.3$ MeV. The data allow us to test various aspects of the model separately: at 12.4 MeV/nucleon the modeling of the pre-equilibrium LP emission and the decay of the CN by LP evaporation is tested, at 19.7 MeV/nucleon the effects of a breakup-fusion process, and at 30.0 MeV/nucleon the concept of a limiting excitation energy.

ACKNOWLEDGMENTS

We would like to thank the accelerator staff of KVI and the staff of SARA for providing us with the Si beams. This work was part of the research program of the "Stichting voor Fundamenteel Onderzoek der Materie" (FOM), with financial support from the "Nederlandse Organisatie voor Wetenschappelijk Onderzoek" (NWO) and the National Science Foundation.

*Present address: PTT Research, Groningen, The Netherlands.

†On leave from the Institute of Experimental Physics, University of Warsaw, Poland; Present address: Department of Physics, Smith College, Northhampton, Massachusetts 01063.

‡On leave from the Institute of Experimental Physics, University of Warsaw, Poland.

[1] C. Gregoire and B. Tamain, Ann. Phys. **11**, 323 (1986).

[2] Proceedings of the Symposium on Central Collisions, and Fragmentation Processes, edited by C. K. Gelbke [Nucl. Phys. **A471** (1987)].

[3] G. Peilert, A. Rosenhauer, J. Aichelin, H. Stöcker, and W. Greiner, Phys. Rev. C **39**, 1402 (1989).

[4] W. A. Friedman, Phys. Rev. Lett. **40**, 2055 (1989).

[5] H. M. Xu, W. G. Lynch, P. Danielewicz, and G. Bertsch, Michigan State University Report No. MSUCL-724.

[6] K. A. Griffioen, B. J. Gluckman, R. J. Meijer, P. Decowski, and R. Kamermans, Phys. Rev. C **40**, 1647 (1989).

[7] R. J. Meijer, G. J. van Niewenhuizen, A. van den Brink, P. Decowski, K. A. Griffioen, and R. Kamermans, Nucl. Instrum. Methods A **264**, 285 (1988).

[8] R. J. Meijer, A. P. de Haas, J. J. Langerak, C. J. Oskamp,

W. Smit, M. Voerman, P. Decowski, K. A. Griffioen, G. J. van Nieuwenhuizen, and R. Kamermans, Nucl. Instrum. Methods A **265**, 511 (1988).
[9] R. J. Meijer, Ph.D. thesis, University of Utrecht, 1989 (unpublished).
[10] E. A. Bakkum, A. van den Brink, R. J. Meijer, and R. Kamermans, Nucl. Instrum. Methods A **243**, 435 (1986).
[11] A. J. Michielsen and P. Decowski, Nucl. Instrum. Methods A **282**, 121 (1989).
[12] P. Decowski, E. A. Bakkum, P. F. Box, K. A. Griffioen, R. Kamermans, and R. J. Meijer, Phys. Rev. C **37**, 2495 (1988).
[13] F. Pühlhofer, Nucl. Phys. **A280**, 267 (1977).
[14] M. F. Vineyard, J. S. Bauer, C. H. Gosdin, R. S. Trotter, D. G. Kovar, C. Beck, D. J. Henderson, R. V. F. Janssens, B. D. Wilkins, P. Chowdhury, H. Ikezoe, W. Kuhn, J. J. Kolata, J. D. Hinnefeld, C. F. Maguire, J. F. Mateja, F. W. Prosser, and G. S. F. Stephans, Phys. Rev. C **41**, 1005 (1990).
[15] W. W. Wilcke, J. R. Birkelund, H. J. Wollersheim, A. D. Hoover, J. R. Huizenga, W. U. Schröder, and L. E. Tubbs, At. Data Nucl. Data Tables **25**, 389 (1980).
[16] R. J. Charity, M. A. McMahan, G. J. Wozniak, R. J. McDonald, L. G. Moretto, D. G. Sarantites, L. G. Sobotka, G. Guarino, A. Pantaleo, L. Fiore, A. Gobbi, and K. D. Hildenbrand, Nucl. Phys. **A483**, 371 (1888).
[17] J. Blachot, J. Crançon, B. De Concourt, A. Gizon, A. Lleres, and H. Nifenecker, in *Proceedings of the XXIII International Winter Meeting on Nuclear Physics, Bormio, 1985,* edited by I. Iori (Ricerca Scientifica ed Educazione Permanente, Milano, 1985), p. 598.
[18] M. Conjeaud, S. Harar, M. Mostefai, C. E. Pollaco, C. Volant, Y. Casagnou, R. Dayras, R. Legrain, H. Oeschler, and Y. Saint-Laurant, Phys. Lett. **159B**, 374 (1984).
[19] G. Auger, E. Plagnol, D. Jouan, C. Guet, D. Heuer, M. Maurel, H. Nifenecker, C. Ristori, F. Schussler, H. Doubre, and C. Gregoire, Phys. Lett. **169B**, 161 (1986).
[20] D. X. Jiang, H. Doubre, J. Galin, D. Guerreau, E. Piasecki, J. Pouthas, A. Sokolov, B. Cramer, G. Ingold, U. Jahnke, E. Schwinn, J. L. Charvet, J. Frehaut, B. Lott, C. Magnago, M. Morjean, Y. Pattin, Y. Pranal, J. L. Uzureau, B. Gatty, and D. Jaquet, Nucl. Phys. **A503**, 560 (1989).
[21] S. Levit and P. Bonche, Nucl. Phys. **A437**, 426 (1985).
[22] K. A. Griffioen, E. A. Bakkum, P. Decowski, R. J. Meijer, and R. Kamermans, Phys. Rev. C **37**, 2502 (1988).
[23] MINUIT, CERN library routine.
[24] W. Rösch, A. Richter, G. Schrieder, R. Gentner, K. Keller, L. Lassen, W. Lücking, R. Schrek, W. Cassing, and H. Gemmeke, Phys. Lett. B **197**, 17 (1987).
[25] W. Cassing, Z. Phys. A **329**, 471 (1988).
[26] W. Cassing, Z. Phys. A **327**, 87 (1988).
[27] W. A. Friedman, Phys. Rev. C **27**, 27 (1983).
[28] H. Homeyer, M. Burgel, Ch. Egelhaaf, H. Fuchs, and G. Thoma, Z. Phys. A **319**, 143 (1984).
[29] K. Möhring, W. J. Swiatecki, and M. Zielinska-Pfabe, Nucl. Phys. **A440**, 89 (1985).
[30] A. S. Goldhaber, Phys. Lett. **53B**, 306 (1974).
[31] M. J. Murphy, Phys. Lett. **135B**, 25 (1984).
[32] P. L. Gonthier, H. Ho, M. N. Namboodiri, J. B. Natowitz, L. Adler, S. Simon, K. Hagel, S. Kniffen, and A. Khodai, Nucl. Phys. **A411**, 289 (1983).
[33] K. A. Griffioen, R. J. Meijer, P. F. Box, P. Decowski, G. J. van Nieuwenhuizen, R. Kamermans, H. W. Wilschut, A. Giorni, C. Morand, A. Demeyer, and D. Guinet, Phys. Lett. B **237**, 24 (1990).
[34] A. Gilbert, F. S. Chen, and A. G. W. Cameron, Can. J. Phys. **43**, 1248 (1965); A. Gilbert and A. G. W. Cameron, *ibid.* **43**, 1446 (1965).
[35] K. L. Le Couteur and D. W. Lang, Nucl. Phys. **13**, 32 (1959).
[36] D. W. Lang, Nucl. Phys. **53**, 113 (1964).
[37] E. A. Bakkum, P. Decowski, K. A. Griffioen, R. J. Meijer, and R. Kamermans, Nucl. Phys. **A511**, 117 (1990).
[38] R. J. Meijer, P. F. Box, P. Decowski, K. A. Griffioen, R. Kamermans, G. J. Nieuwenhuizen, H. W. Wilschut, A. Giorni, C. Morand, A. Demeyer, and D. Guinet, in *Proceedings of the XXVII International Winter Meeting on Nuclear Physics, Bormio, 1989,* edited by I. Iori (Ricerca Scientifica ed Educazione Permanente, Milano, 1989), p. 203.
[39] J. R. Huizenga, A. N. Behkami, I. M. Govil, W. U. Schröder, and J. Toke, Phys. Rev. C **40**, 668 (1989).
[40] W. Rösch, P. von Neumann-Cosel, A. Richter, G. Schrieder, R. Gentner, L. Lassen, and H. W. Wilschut, Nucl. Phys. **A509**, 615 (1990).